

EXPERTNET: A Symbiosis of Classification and Clustering

Shivin Srivastava¹, Kenji Kawaguchi¹ and Vaibhav Rajan¹

¹ National University of Singapore
{shivin, kenji, vaibhav}@comp.nus.edu.sg

Abstract

A widely used paradigm to improve the generalization performance of high-capacity neural models is through the addition of auxiliary unsupervised tasks during supervised training. Tasks such as similarity matching and input reconstruction have been shown to provide a beneficial regularizing effect by guiding representation learning. Real data often has complex underlying structures and may be composed of heterogeneous subpopulations that are not learned well with current approaches. In this work, we design **EXPERTNET**, which uses novel training strategies to learn clustered latent representations and leverage them by effectively combining cluster-specific classifiers. We theoretically analyze the effect of clustering on its generalization gap, and empirically show that clustered latent representations from **EXPERTNET** lead to disentangling the intrinsic structure and improvement in classification performance. **EXPERTNET** also meets an important real-world need where classifiers need to be tailored for distinct subpopulations, such as in clinical risk models. We demonstrate the superiority of **EXPERTNET** over state-of-the-art methods on 6 large clinical datasets, where our approach leads to valuable insights on group-specific risks.

1 Introduction

Overfitting is a common problem in high-capacity models, such as neural networks, that adversely affects generalization performance. A standard approach to reduce overfitting is regularization. Various regularization strategies have been developed such as those based on norm penalties and some specifically designed for neural networks such as dropout and early stopping [Goodfellow *et al.*, 2016]. The use of auxiliary tasks have also been explored for regularization. The rationale comes from multi-task learning, which is known to improve generalization through improved statistical strength via shared parameters [Baxter, 1995; Caruana, 1997].

Since there is no dependence on label acquisition, several unsupervised auxiliary tasks have been explored for regularizing neural networks. Input reconstruction is a common

choice, often implemented using autoencoder-like architectures, e.g. [Rasmus *et al.*, 2015; Zhao, 2015; Zhang *et al.*, 2016; Le *et al.*, 2018]. Such reconstruction-based regularization has the advantage of yielding hidden layer representations closer to the original data topology.

Real data, however, contains complex underlying structures like clusters and intrinsic manifolds that are not disentangled by the bottleneck layer of autoencoders. This has been studied in the context of purely unsupervised models that have explored the joint tasks of clustering and dimensionality reduction (DR) to find “cluster-friendly” representations. E.g., in [Yang, 2017], it is shown that joint clustering and DR outperforms the disassociated approach of independently performing DR followed by clustering. Recognizing the importance of preserving cluster structure in latent embedded spaces, we hypothesize that, in addition to reconstruction, clustering-based regularization could improve generalization performance in supervised models.

Our work is also motivated by the need to develop models tailored to distinct subpopulations in the data. This is a common requirement in clinical risk models since patient populations can show significant heterogeneity. Most previous works adopt a ‘cluster-then-predict’ approach to model such data e.g., [Ibrahim *et al.*, 2020], where clustering is first done independently to find subpopulations (called subtypes) and then predictive models for each of these clusters are learnt. Such subtype-specific models are often found to outperform models learnt from the entire population [Masoudnia and Ebrahimpour, 2014]. They also provide a form of interpretability and subsequent clinical decisions can be personalized to each patient group’s characteristics. However, in these approaches, clustering is performed independent of classifier training, and may not discover latent structures that are beneficial for subsequent classification. This leads us to hypothesize that combined clustering with supervised classification will lead to better performance compared to such cluster-then-predict approaches.

We thus design **EXPERTNET**, a deep learning model that performs simultaneous clustering and classification. **EXPERTNET** consists of components that have both local and global view of the data space. The local units specialize in classifying observations in clusters found in the data while the global unit is responsible for generating cluster friendly embeddings based on the feedback given by local units. Apart

from being a supervised model, EXPERTNET can function as an unsupervised model that can perform target-specific clustering. In summary, our contributions are:

1. **Model:** We design EXPERTNET, a neural model for simultaneous clustering and classification with cluster-specific local networks. We introduce novel training strategies to obtain latent clusters and use them effectively to improve generalization of the classifiers.
2. **Theoretical Guarantees:** We analyze the effect of clustering on EXPERTNET’s generalization gap.
3. **Experiments:** Our extensive experiments demonstrate the efficacy of our model over both reconstruction-based regularization and cluster-then-predict approaches. On 6 large real-world clinical datasets EXPERTNET achieves clustering performance that is comparable to, and achieves classification performance that is considerably better than, state-of-the-art methods.

2 Background and Related Work

Unsupervised learning techniques are often used to pretrain a neural network before finetuning with supervised tasks [Bengio *et al.*, 2007]. Input reconstruction is commonly used to regularize deep models. [Zhang *et al.*, 2016] jointly train a supervised neural model with an unsupervised reconstruction network. [Zhao, 2015] showed that by adding decoding pathways, to add an auxiliary reconstruction task to the objective, improves the performance of supervised networks. Similarly [Le *et al.*, 2018] append a prediction layer to the embedding layer to improve generalization performance.

A more dissociated way of using clustering to benefit supervised models is to simply find clusters in the data and then train separate models on each of them that. Amongst such techniques, there are some algorithms [Finley and Joachims, 2008; Gu and Han, 2013; Fu *et al.*, 2010] that impose a common, global regularization scheme on all the individual classifiers. In some other works [Reyna *et al.*, 2019; Lasko *et al.*, 2013; Suresh *et al.*, 2018], all the individual classifiers are completely independent. Such analysis is common in clinical data where patient stratification is done followed by predictive modeling. E.g., Deep Mixture Neural Networks (DMNN) [Li *et al.*, 2020b], designed with this aim, is based on an autoencoder architecture while having an additional gating network, which is first trained to learn clusters through k -means. Local networks corresponding to each cluster are trained using a weighted combination of losses, where the weights are determined by the gates.

Simultaneous clustering and representation learning have been used in purely unsupervised settings. Examples include neural clustering models such as Deep Embedded Clustering (DEC) [Xie *et al.*, 2016] and Improved DEC (IDEC) [Guo *et al.*, 2017] and Deep Clustering Network (DCN) [Yang, 2017]. Recent self-supervised learning techniques also employ cluster centroids as pseudo class labels in embedded data space to improve the quality of representations [Li *et al.*, 2020a; Caron *et al.*, 2018].

We briefly describe DEC [Xie *et al.*, 2016] as the loss function in EXPERTNET is based on their formulation. Their key idea is to find latent representations z_i for data points using an

autoencoder by first pretraining it. Initial cluster centers $\{\mu_j\}$ are obtained by using k -means on the latent representations. The decoder is then removed and the representations are fine tuned by minimizing the loss function:

$$L_c = KL(P||Q) = \sum_{i=1}^N \sum_{j=1}^N p_{ij} \log \frac{p_{ij}}{q_{ij}} \quad (1)$$

where q_{ij} is the probability of assigning the i^{th} data point (z_i) to the j^{th} cluster (with centroid μ_j) measured by the Student’s t -distribution [V. D. Maaten and Hinton, 2008] as:

$$q_{ij} = \frac{(1 + \|z_i - \mu_j\|^2)^{-1}}{\sum_j (1 + \|z_i - \mu_j\|^2)^{-1}} \quad (2)$$

The target distribution p_{ij} is defined as

$$p_{ij} = \frac{q_{ij}^2 / \sum_i q_{ij}}{\sum_j (q_{ij}^2 / \sum_i q_{ij})} \quad (3)$$

The predicted label of x_i is $\text{argmax}_j q_{ij}$. Minimizing the loss function L_c is a form of self-training as points with high confidence act as anchors and distribute other points around them more densely.

DEC, IDEC and DCN are all centroid-based and have objectives similar to that of k -means. In such approaches, the encoder can map the centroids to a single point to make the loss zero and thus collapse the clusters. Hence, previous methods employ various heuristics to balance cluster sizes, e.g., through sampling approaches [Caron *et al.*, 2018] or use of priors [Jitta and Klami, 2018].

3 EXPERTNET

Given N datapoints $\{x_i \in X\}_{i=1}^N$, and class labels $y_i \in \{1, \dots, \mathcal{B}\}$, associated with every point x_i , our aim is to simultaneously (i) cluster the N datapoints into k clusters, each represented by a centroid $\mu_j, j \in \{1, \dots, k\}$, and (ii) build k distinct supervised classification models within each cluster to predict the class labels. Note that during training, labels are used only for building the classification models and not for clustering.

Network Architecture

Fig. 1 shows the neural architecture of EXPERTNET that consists of an encoder, a decoder and k local networks (LN_j). The encoder $f(\mathcal{U}) : X \rightarrow Z$ is used to obtain low-dimensional representations of the input datapoints. Cluster structure is learnt in this latent space and representations in each cluster are used in local networks, $h(\mathcal{W}_j) : Z \rightarrow \hat{y}_j$ for $j = 1 \dots k$ to train k classification models. In addition, there is a decoder $g(\mathcal{V}) : Z \rightarrow X$ that is used to reconstruct the input from the embeddings. EXPERTNET is parameterized by three sets of weights: $\mathcal{U}, \mathcal{V}, \{\mathcal{W}_j\}_{j=1}^k$ which are learnt by optimizing a combination of losses as described below.

Loss Function

The overall loss function L is a weighted combination, with coefficients $\beta, \gamma > 0$, of the reconstruction loss L_r , clustering loss L_c , cluster balance loss L_{bal} and classification loss L_s :

$$L = L_r + \beta \cdot L_c + \gamma \cdot L_s + \delta \cdot L_{bal} \quad (4)$$

L_c is defined as the KL divergence loss (Eq. 1), where the cluster membership distribution Q (Eq. 2) uses repre-

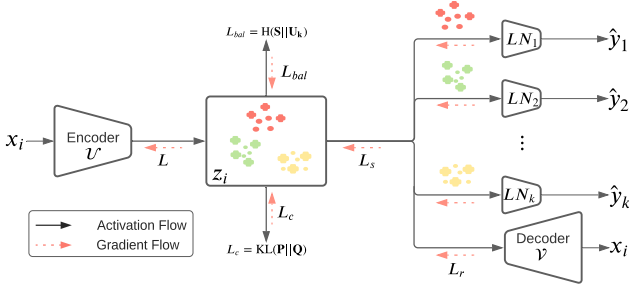


Figure 1: EXPERTNET Architecture

representations z_i and cluster centroids μ_j inferred during EXPERTNET training. As suggested in [Guo *et al.*, 2017; Yang, 2017], to prevent distortion in the latent space and improve clustering performance, we add the reconstruction loss measured by mean squared error:

$$L_r = \sum_{i=1}^N \|x_i - g(f(x_i))\|^2 \quad (5)$$

We design a novel cluster balance loss to discourage unevenly distributed cluster sizes. We define the ‘soft’ size of a cluster C_j as $|C_j| = \sum_i q_{ij}$ and cluster support counts $\mathbf{S} = [|\mathcal{C}_1|, |\mathcal{C}_2|, \dots, |\mathcal{C}_k|]$ as a k -dimensional probability distribution. Let $\mathbf{U}_k = (1/k)\mathbf{U}(0, 1)$ denote the k -dimensional uniform distribution function. We use the Hellinger distance (H), which measures the dissimilarity between two distributions, as the loss $L_{bal} = H(\mathbf{S}||\mathbf{U}_k) = \frac{1}{2}\|\sqrt{\mathbf{S}} - \sqrt{\mathbf{U}_k}\|_2$. L_s is a weighted cross entropy loss described in the following.

EXPERTNET Training

To initialize the parameters $(\mathcal{U}, \mathcal{V})$, we first pre-train the encoder and decoder with the input data using only the reconstruction loss L_r . This is followed by k -means clustering on $\{z_i = f(x_i; \mathcal{U})\}_{i=1}^N$ to obtain cluster centroids $\{\mu_i\}_{i=1}^k$ which are used to calculate cluster membership and target distributions, Q, P . After initialization, we use mini-batch Stochastic Gradient Descent to train the entire network, using the loss L (details are in Appendix E). To stabilize training we update P only after every epoch.

Since the embeddings get updated progressively in every iteration, we train the LNs for a larger number of *sub-iterations* within every iteration of the main training loop. The number of sub-iterations gradually increases (1 per every 5 epochs until a max-limit we set to 10). This enables the LNs to learn better from the stabilized clustered embeddings than from the intermediate representations.

Further, we design a novel strategy called *stochastic cohort sampling* used in each sub-iteration, which leads to more robust classifiers, as verified in our experiments. Instead of training each LN with a fixed cluster of data points (e.g., using $\text{argmax}_{j=1}^k q_{i,j}$), we leverage the probabilistic definition of clusters to obtain multiple, different cluster assignments for the same set of embeddings. Considering q_i , the i^{th} row of Q , as a cluster probability distribution for z_i , we sample a random variable s_i from q_i , denoting the cluster assignment for the point x_i . We can define a cluster realization

Algorithm 1: ExpertNet Training

Input: Training Data: $X \in \mathbb{R}^{n \times d}$, labels $y^{n \times 1} \in [\mathcal{B}]^n$, $k, f(\cdot; \mathcal{U}), g(\cdot; \mathcal{V})$ and $\{h_j(\cdot; \mathcal{W}_j)\}_{j=1}^k, \mathcal{J}$

- 1 \triangleright **Initialization**
- 2 Pre-train $f(\cdot; \mathcal{U})$ & $g(\cdot; \mathcal{V})$ via back-propagating loss in eq. 5
- 3 Compute $\mu(C_j) \forall C_j$ s.t. $j \in [k]$ and $b \in [\mathcal{B}]$
- 4 Compute matrices Q and P according to eqs. 2 and 3
- 5 \triangleright **Algorithm**
- 6 **while** Validation AUC increases **do**
- 7 **for** every mini-batch \mathcal{X}_b **do**
- 8 $\mathcal{Z}_b \leftarrow f(\mathcal{X}_b; \mathcal{U})$
- 9 Calculate Q_b by eq. (2)
- 10 **for** T sub-iterations **do**
- 11 Sample $\{s_i \sim q_i\}_{i=1}^{|\mathcal{X}_b|}$
- 12 Calculate $\{\mathcal{X}_m = \{x_i : s_i = j\}_{i=1}^{|\mathcal{X}_b|}\}_{j=1}^k$
- 13 Train local classifiers $\{h_j\}_{j=1}^k$ on $(\mathcal{X}_j, \mathcal{Y}_j)$
- 14 Update $\{\mathcal{W}_j\}_{j=1}^k$
- 15 Backpropagate
 $L = L_r + \beta \cdot L_c + \gamma \cdot L_s + \delta \cdot L_{bal}$ and
update $\mu, \mathcal{U}, \mathcal{V}$ and \mathcal{W}
- 16 Update P via eq. (3)
- 17 \triangleright **Fine tune Local Classifiers**
- 18 For every cluster C_j , train a classifier f_j on $(\mathcal{X}_j, \mathcal{Y}_j)$.
- 19 **Output** Trained EXPERTNET model. Cluster centroids $\mu = \{\mu_j\}_{j=1}^k$

$C_m = \{i : s_i = m\}_{i=1}^N$ (i.e. index of all the points assigned to cluster C_m) and $\mathcal{X}_m = \bigcup_{j \in C_m} \{x_j\}$. The LNs are trained

on these cluster realizations for $T - 1$ sub-iterations *without* backpropagating the error to the encoder. The individual errors are collected from all the k LNs only at the last (T^{th}) iteration and backpropagated to the encoder to adjust the cluster representations accordingly. The final classification loss is a weighted cross entropy (CE) loss:

$$L_s = \sum_{j=1}^k \sum_{p \in C_j} q_{p,j} \text{CE}(y_p, h_j(x_p; \mathcal{V}_j)). \quad (6)$$

After training, the encoder network is frozen and the local networks are finetuned on the latent embeddings via stochastic cohort sampling to further improve LN performance.

EXPERTNET Prediction

Prediction can be done using the encoder and local networks. For a test point \hat{x}_p , the soft cluster probabilities (\hat{q}_{pj}) are calculated from Eq. 2. All the local networks (see stochastic cohort sampling above) can be used to predict the class label $\hat{y}_p = \sum_{j=1}^k \hat{q}_{pj} h_j(\hat{x}_p)$.

4 Theoretical Analysis

Let $\{\Omega_j\}_{j=1}^k$ be a partition of \mathcal{X} such that $\mathcal{X} = \cup_{j=1}^k \Omega_j$ where $\Omega_j \cap \Omega_{j'} = \emptyset$ for $j \neq j'$. This corresponds to the

inverse image of clustering at the space of z . We define N_j as

$$N_j = \sum_{i=1}^N \mathbb{1}\{x_i \in \Omega_j\}; f(x) = \sum_{j=1}^k \mathbb{1}\{x \in \Omega_j\} f_j(x)$$

where $f_j = g_j \circ f$ with g_j being the encoder for the cluster Ω_j and f being the shared encoder.

While we provide the results for multi-class classification in Appendix A, this section considers binary classification. For binary classification problems with $y \in \{-1, +1\}$ and $f(x) \in \mathbb{R}$, define the margin loss as follows:

$$\ell_\rho(f(x), y) = \ell_\rho^{(1)}(f(x)y)$$

where

$$\ell_\rho^{(1)}(q) = \begin{cases} 0 & \text{if } \rho \leq q \\ 1 - q/\rho & \text{if } 0 \leq q \leq \rho \\ 1 & \text{if } q \leq 0. \end{cases}$$

Define the 0-1 loss as:

$$\ell_{01}(f(x), y) = \mathbb{1}\{f(x)y \leq 0\}.$$

To simplify the equation and discussion, we consider the case where $\Pr(x \in \Omega_j) = 1/k$ (uniform) and $N_j = N/k$ (uniform), whereas the results for a more general case are presented in the appendix. Defining $\hat{\mathbb{E}}_{x,y}[\ell_\rho(f(x), y)]$ to denote the empirical los, we have:

Theorem 1. *Suppose that for all $j \in \{0, \dots, k\}$, the function σ_l^j is 1-Lipschitz and positive homogeneous for all $l \in [\max(L-1, Q-1)]$ and $\|x^j\| \leq B_j$ for all $x^j \in \Omega_j$. Let $\mathcal{F}_j = \{x \in \Omega_j \mapsto (g_j \circ e)(x) : (\forall l \in [L-1])[\|W_l^j\|_F \leq M_l^j \wedge \|W_l^0\|_F \leq M_l^0]\}$ and $\mathcal{F}^k = \{x \mapsto f(x) : f(x) = \sum_{j=1}^k \mathbb{1}\{x \in \Omega_j\} f_j(x), f_j \in \mathcal{F}_j\}$. Then, for any $\delta > 0$, with probability at least $1 - \delta$ over an i.i.d. draw of m i.i.d. test samples $((x_i, y_i))_{i=1}^m$, the following holds: for all maps $f^k \in \mathcal{F}^k$,*

$$\begin{aligned} \mathbb{E}_{x,y}[\ell_{01}(f^k(x), y)] - \hat{\mathbb{E}}_{x,y}[\ell_\rho(f^k(x), y)] \leq \\ \zeta_1 \left(\frac{\sum_{j=1}^K B_j \prod_{l=1}^L M_l^j}{\sqrt{kN}} \right) \\ + 3\sqrt{\frac{k \ln(2k/\delta)}{2N}} \end{aligned}$$

where $\zeta_1 = 2\rho^{-1}(\sqrt{2 \log(2)(L+Q)} + 1)(\prod_{l=1}^Q M_l^0)$ is a k independent term.

The proof is presented in Appendix A. Theorem 1 shows the generalization bound with the following:

- Increasing k can reduce the empirical loss $\mathbb{E}_{x,y}[\ell_\rho(f^k(x), y)]$ (since it increases the expressive power), resulting in a tendency for a better expected error $\mathbb{E}_{x,y}[\ell_{01}(f^k(x), y)]$.
- Increasing k increases the last term $\sqrt{\frac{k \ln(2k/\delta)}{2N}}$, resulting in a tendency for a worse expected error $\mathbb{E}_{x,y}[\ell_{01}(f^k(x), y)]$.
- Increasing k can reduce the complexity term $\frac{(\sum_{j=1}^k B_j \prod_{l=1}^L M_l^j)}{\sqrt{kN}}$ (since (1) each sub-network only needs to learn a simpler classifier with larger k , resulting in a smaller value of $\prod_{l=1}^L M_l^j$; (2) each domain decrease and

hence B_j decrease as k increase), resulting in a tendency for a better expected error $\mathbb{E}_{x,y}[\ell_{01}(f^k(x), y)]$.

Not surprisingly, the generalization gap is inversely dependent on N , the total number of data points, indicating that more observations will lead to a more accurate model. There is no simple relationship between k suggesting that the best number of clusters might have to be found empirically.

5 Experiments

We evaluate the classification and clustering performance of EXPERTNET on 6 large clinical datasets. We analyze EXPERTNET through an ablation study and investigate its sensitivity to model hyperparameters. Finally, we present a case study that illustrates its utility in clinical risk modeling.

5.1 Data

We use 6 large clinical datasets; Table 1 lists the number of observations and features in each of them. WID data is from the Women In Data Science challenge [Lee et. al., 2020] to predict patient mortality. Diabetes data is from the UCI Repository where the task is readmission prediction. All the remaining datasets have data from the MIMIC III ICU Database [Fei et al., 2020]. CIC and Sepsis have been used for mortality and sepsis prediction challenges in Physionet [Silva, 2012; Reyna et. al., 2019]. Kidney and Respiratory data has been extracted by us for the tasks of Acute Kidney Failure and Acute Respiratory Distress Syndrome prediction. All the above tasks are posed as binary classification problems. We also derive a multiclass dataset (CIC-LOS) from the CIC dataset where we predict Length of Stay (LOS), discretized into 3 classes (based on 3 quartiles). We consider a random 57-18-25 split to create training, validation and testing splits in each dataset. More details of data preprocessing and feature extraction are in Appendix D.

Dataset	#Instances	#Features	MAJ
WID Mortality [Lee et. al., 2020]	91711	241	0.91
Diabetes [Lichman., 2013]	100000	9	0.54
Sepsis [Reyna et. al., 2019]	40328	89	0.93
Kidney [Fei et al., 2020]	14087	89	0.51
Respiratory [Fei et al., 2020]	22477	89	0.92
CIC [Silva, 2012]	12000	117	0.85
CIC-LOS	12000	116	3 classes

Table 1: Summary of datasets. MAJ: proportion of majority class instances (for binary labels).

5.2 Classification and Clustering Performance

Baselines

As baselines for the classification task, we use 3 different kinds of techniques. The first is a feedforward neural network (**baseline**) that only performs classification. It's architecture is set to be identical to that of a combination of EXPERTNET's encoder and a single local network. The second is the Supervised Autoencoder (SAE) [Le et al., 2018] that uses reconstruction loss as an unsupervised regularizer (similar architecture as **baseline**). The third category uses the common 'cluster-then-predict' approach, where clustering is in-

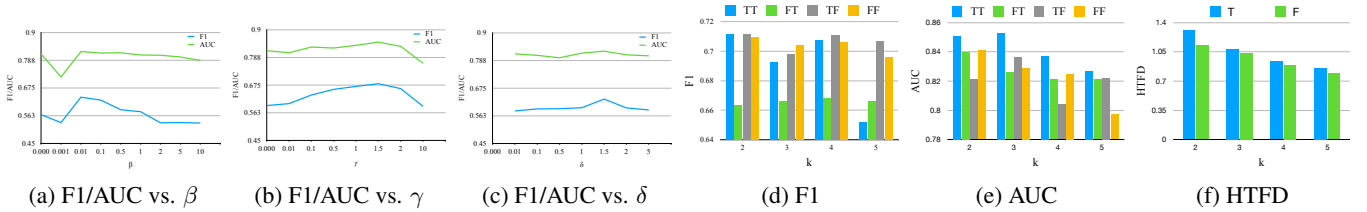


Figure 2: Sensitivity Analysis (a-c) and Ablation Studies (d-f) on the CIC dataset

Dataset	k	HTFD					AUC						
		KMeans	DCN	IDEC	DMNN	EXPERTNET	Baseline	SAE	KMeans-Z	DCN-Z	IDEC-Z	DMNN	EXPERTNET
CIC	1	-	-	-	-	-	0.628	0.693	0.804	0.819	0.817	0.721	0.835
	2	1.125	NA	1.175	1.233	1.302			0.705	NA	0.787	0.784	0.851
	3	1.072	NA	1.081	1.173	1.082			0.63	NA	0.817	0.799	0.853
	4	0.992	NA	0.971	1.107	0.934			0.593	NA	0.811	0.808	0.837
Sepsis	1	-	-	-	-	-	0.654	0.681	0.823	0.772	0.823	0.670	0.908
	2	1.347	1.365	1.406	1.476	1.283			0.598	0.679	0.806	0.767	0.909
	3	1.455	1.376	1.301	1.351	1.319			0.58	0.725	0.772	0.794	0.899
	4	1.357	NA	1.361	1.333	1.301			0.55	NA	0.804	0.829	0.904
AKI	1	-	-	-	-	-	0.584	0.552	0.601	0.591	0.613	0.617	0.694
	2	1.108	1.014	1.11	0.760	1.044			0.44	0.601	0.585	0.690	0.69
	3	1.164	1.166	1.166	0.803	1.168			0.467	0.582	0.57	0.689	0.67
	4	1.148	1.14	1.141	0.767	1.172			0.439	0.601	0.596	0.691	0.646
ARDS	1	-	-	-	-	-	0.612	0.631	0.726	0.661	0.722	0.601	0.768
	2	1.25	1.228	1.283	0.581	1.312			0.628	0.676	0.638	0.758	0.73
	3	1.17	NA	1.171	1.156	1.282			0.644	NA	0.666	0.766	0.708
	4	1.154	NA	1.119	1.114	1.262			0.616	NA	0.635	0.697	0.744
WID-M	1	-	-	-	-	-	0.711	0.703	0.853	0.814	0.853	0.686	0.883
	2	1.285	1.23	1.571	1.438	1.534			0.731	0.739	0.8	0.846	0.883
	3	1.328	NA	1.501	1.404	1.514			0.709	NA	0.809	0.853	0.874
	4	1.41	NA	1.388	1.363	1.469			0.691	NA	0.806	0.865	0.859
Diabetes	1	-	-	-	-	-	0.566	0.551	0.58	0.574	0.582	0.578	0.587
	2	1.633	1.554	1.707	1.663	1.802			0.53	0.566	0.567	0.581	0.587
	3	1.593	1.53	1.698	1.245	1.67			0.514	0.568	0.563	0.579	0.585
	4	1.611	1.398	1.578	1.381	1.609			0.507	0.569	0.563	0.581	0.586
CIC-LOS	1	-	-	-	-	-	0.646	0.659	0.652	0.639	0.642	-	0.663
	2	1.042	1.003	1.148	-	1.101			0.575	0.632	0.648	-	0.672
	3	1.038	0.99	1.052	-	0.925			0.567	0.636	0.642	-	0.664
	4	0.995	NA	0.955	-	0.871			0.539	NA	0.64	-	0.664

Table 2: Clustering and Classification performance. Best values in bold. NA indicates no results due to an empty cluster. Note that HTFD values are not defined for $k = 1$.

independently performed first and classifiers are trained on each cluster (denoted by **-Z**). In this category, we compare with 3 clustering methods **k-means** (where we use an autoencoder to get embeddings which are then clustered using k -means), Deep Clustering Network **DCN** [Yang, 2017] and Improved Deep Embedded Clustering (**IDEC**) [Guo *et al.*, 2017]. We also use Deep Mixture Neural Networks (**DMNN**) [Li *et al.*, 2020b] that follows this paradigm. Note that their implementation only supports binary classification. We use stochastic cohort sampling during prediction in all baselines that use clustering for a fair comparison. We compare the clustering performance obtained by **EXPERTNET** with that of **DMNN**, k -means, **DCN** and **IDEC**.

Performance Metrics

Standard classification metrics, Area Under the Receiver Operating Characteristic (AUC) and F1 scores, are used for binary classification. For multiclass setting, we use one-vs-rest algorithm to calculate AUC.

To evaluate clustering we use Silhouette scores and another score, HTFD, described below, that evaluates feature discrimination in the inferred clusters. A common practice in clustering studies (e.g., [Li *et al.*, 2015]) is to check, for each feature, if there is a statistically significant difference in its distribution across the clusters. A low p-value (< 0.05) indicates significant difference. To aggregate this over all features F , we define, for each cluster in a clustering, the metric **Hypothesis Testing based Feature Discrimination (HTFD)**:

$$\text{HTFD}(C_i) = \frac{1}{|F|} \sum_{f \in F} -\ln(\text{p-value}(X_i^f, X^f)) * 0.05$$

where X_i^f denotes the values of feature f for data points in cluster C_i and X^f denotes the feature values of data points in all clusters except C_i . Student's t-test is used to obtain the p-value. The negative logarithm of p-value is multiplied by the significance level, to normalize and obtain a measure

wherein higher values indicate better clustering. To obtain an overall value for the entire clustering, we take the average of individual, cluster-wise HTFD values.

Hyperparameter Settings

For **DCN-Z** and **IDEC-Z**, we use default parameters as suggested by their authors. For **EXPERTNET** we let $(\beta, \gamma, \delta) = (0.5, 1.5, 1)$. We select these default values by considering the sensitivity analysis (see Fig. 2). The common encoder has layers of size 128-64-32 and local expert network has layers of size 64-32-16-8. The size of latent embeddings is 20. We evaluate all the methods for four different values of $K = 1, 2, 3, 4$.

Results

Table 2 shows the performance of all methods compared, on classification and clustering. We observe that cluster-then-predict methods (***-Z**) and **DMNN** generally perform better than **SAE**, which suggests that clustering-based regularization is more effective than reconstruction-based regularization. **SAE** outperforms the baseline on most datasets. These results align with previous research that show that unsupervised regularization aids supervised learning. **EXPERTNET** outperforms all methods on all datasets for at least one input cluster size. Also note that **EXPERTNET**'s performance does not degrade with increasing number of clusters as seen for **KMeans-Z**. Overall, for classification, **EXPERTNET** consistently outperforms all the baselines on all datasets.

With respect to clustering, the performance of **EXPERTNET** is superior to the best baseline in 5 datasets, for some values of k . For other values of k , and on other datasets, the performance values are comparable or lower. F1 scores and Silhouette scores are in Appendix B, where the performance trends are similar. Overall, the results show that **EXPERTNET** achieves clustering performance that is comparable to, and achieves classification performance that is considerably better than, the state-of-the-art alternatives respectively.

5.3 Sensitivity Analysis and Ablation Studies

We evaluate the effect of hyperparameters β, γ and δ on **EXPERTNET**. We individually vary each hyperparameter while setting other two to 0 and measure the classification performance. Figures 2a, 2b and 2c show the results for the **CIC** dataset. We observe that both the F1 and AUC values are fairly robust to changes in their values.

Our stochastic cohort sampling approach may or may not be used independently during training and prediction. To evaluate its effect we evaluate all four combinations through an ablation study. We denote the combinations by **TT**, **TF**, **FT** and **FF**, where the first and second positions indicate training and prediction respectively. **T** indicates use of our approach while **F** indicates that it is not used. Figure 2d and 2e show the F1 and AUC scores for all 4 combinations on the **CIC** dataset (results on **Sepsis** dataset in Appendix C). The best performance is achieved when the approach is used both in training and prediction (**TT**). For clustering, there is no prediction. Figure 2f shows that the performance is better with rather than without sampling. All the results shown are averages over 5 runs.

$ C_1 = 2458$ $\%D = 0.115$	$ C_2 = 1890$ $\%D = 0.032$	$ C_3 = 2402$ $\%D = 0.254$
Age	Age	GCS_last
GCS_last	UrineOutputSum	BUN_last
BUN_last	GCS_last	Age
RespRate_median	BUN_first	Lactate_last
BUN_first	CSRU	Bilirubin_last
Weight_last	GCS_lowest	Length_of_stay
HR_highest	MechVentDuration	GCS_median
Weight_first	BUN_last	SOFA
Weight	RespRate_median	Weight
RespRate_highest	HR_highest	HCO3_last

Table 3: Important Features for mortality prediction in respective clusters. Features common in all three clusters are highlighted in yellow while those common in two are highlighted in purple. Rest are unique to their respective clusters.

5.4 Case Study: Mortality Prediction

As a case study, we illustrate the use of **EXPERTNET** on the **CIC** mortality prediction data for $k = 3$ clusters. Since clustering is done simultaneously with classification, the clusters are influenced by the target label, i.e., mortality indicator, and thus, by design, **EXPERTNET** is expected to find mortality subtypes. In other words, we expect the inferred clusters to have different risk factors tailored to each underlying subpopulation. To evaluate this, we examine feature importances for each cluster's local risk model. We distil the knowledge of the local networks into a simpler student model [Gou *et al.*, 2021], a Gradient Boosting Classifier, in our case, that provides feature importance values.

In Table 3, we list the cluster sizes C_i , proportion of patients who do not survive ($\%D$) and the top 10 most important features in each cluster. We see that, as expected, the risk models created by **EXPERTNET** deem different sets of features as important for predicting mortality. Out of the 10 most important features, each risk model contains 3 common features, 4, 3 and 1 features common across two models respectively and 3, 4 and 6 features unique to respective clusters. Appendix F presents further analysis of the clusters.

6 Conclusion

We design **EXPERTNET** a model for combined clustering and classification and theoretically analyze its generalization properties. Our model can be viewed as a mixture of expert networks trained on inferred clusters in the data. Our experiments show that both regularization through unsupervised clustering and stochastic sampling strategy during training lead to substantial improvement in classification performance. We demonstrate the efficacy of **EXPERTNET** on several clinical datasets, for predictive modeling tailored to subpopulations inferred from the data.

The clustering performance of **EXPERTNET** is comparable to that of other deep clustering methods and may be improved further. This can be explored in future work along with ways to combine hierarchical clustering algorithms with supervised models and applications in other domains.

References

- [Bartlett and Mendelson, 2002] P. L. Bartlett and S. Mendelson. Rademacher and gaussian complexities: Risk bounds and structural results. *JMLR*, 2002.
- [Bartlett *et al.*, 2017] Peter L Bartlett, Dylan J Foster, and Matus J Telgarsky. Spectrally-normalized margin bounds for neural networks. In *NeurIPS*, 2017.
- [Baxter, 1995] Jonathan Baxter. Learning internal representations. In *Proceedings of the eighth annual conference on Computational learning theory*, pages 311–320, 1995.
- [Bengio *et al.*, 2007] Y. Bengio, P. Lamblin, D. Popovici, and H. Larochelle. Greedy layer-wise training of deep networks. In *NeurIPS*, pages 153–160, 2007.
- [Caron *et al.*, 2018] M. Caron, P. Bojanowski, A. Joulin, and M. Douze. Deep clustering for unsupervised learning of visual features. In *ECCV*, pages 132–149, 2018.
- [Caruana, 1997] Rich Caruana. Multitask learning. *Machine learning*, 28(1):41–75, 1997.
- [Fei *et al.*, 2020] H. Fei, Y. Ren, and D. Ji. Mimic and conquer: Heterogeneous tree structure distillation for syntactic NLP. In *EMNLP 2020*, pages 183–193, Online, November 2020.
- [Finley and Joachims, 2008] T. Finley and T. Joachims. Supervised k-means clustering. 2008.
- [Fu *et al.*, 2010] Zhouyu Fu, Antonio Robles-Kelly, and Jun Zhou. Mixing linear svms for nonlinear classification. *IEEE Transactions on Neural Networks*, 2010.
- [Golowich *et al.*, 2018] Noah Golowich, Alexander Rakhlin, and Ohad Shamir. Size-independent sample complexity of neural networks. In *Conference On Learning Theory*, pages 297–299. PMLR, 2018.
- [Goodfellow *et al.*, 2016] Ian Goodfellow, Yoshua Bengio, and Aaron Courville. *Deep learning*. MIT press, 2016.
- [Gou *et al.*, 2021] J. Gou, B. Yu, S. J. Maybank, and D. Tao. Knowledge distillation: A survey. *International Journal of Computer Vision*, 129(6):1789–1819, 2021.
- [Gu and Han, 2013] Quanquan Gu and Jiawei Han. Clustered support vector machines. In *Artificial Intelligence and Statistics*, 2013.
- [Guo *et al.*, 2017] Xifeng Guo, Long Gao, Xinwang Liu, and Jianping Yin. Improved deep embedded clustering with local structure preservation. In *IJCAI*, 2017.
- [Ibrahim *et al.*, 2020] Zina Ibrahim *et al.* On classifying sepsis heterogeneity in the icu: insight using machine learning. *JAMIA*, 2020.
- [Jitta and Klami, 2018] A. Jitta and A. Klami. On controlling the size of clusters in probabilistic clustering. In *AAAI*, 2018.
- [Johnson, 2012] A. EW *et al.* Johnson. Patient specific predictions in the intensive care unit using a bayesian ensemble. In *CinC*, 2012.
- [Koltchinskii and Panchenko, 2002] V. Koltchinskii and D. Panchenko. Empirical margin distributions and bounding the generalization error of combined classifiers. *The Annals of Statistics*, 30(1):1–50, 2002.
- [Lasko *et al.*, 2013] Thomas A Lasko, Joshua C Denny, and Mia A Levy. Computational phenotype discovery using unsupervised feature learning over noisy, sparse, and irregular clinical data. *PLoS one*, 2013.
- [Le *et al.*, 2018] Lei Le *et al.* Supervised autoencoders: Improving generalization performance with unsupervised regularizers. *NeurIPS*, 31:107–117, 2018.
- [Lee *et al.*, 2020] M. Lee *et al.* WiDS (Women in Data Science) Datathon 2020: ICU Mortality Prediction, 2020.
- [Li *et al.*, 2020a] J. Li, P. Zhou, C. Xiong, and S. Hoi. Prototypical contrastive learning of unsupervised representations. *arXiv preprint arXiv:2005.04966*, 2020.
- [Li *et al.*, 2020b] Xiangrui Li, Dongxiao Zhu, and Phillip Levy. Predicting clinical outcomes with patient stratification via deep mixture neural networks. *AMIA Summits on Translational Science*, 2020.
- [Li *et al.*, 2015] Li Li *et al.* Identification of type 2 diabetes subgroups through topological analysis of patient similarity. *Science translational medicine*, 7(311):311ra174–311ra174, 2015.
- [Lichman., 2013] M. Lichman. Uci repository. *UCI*, 2013.
- [Masoudnia and Ebrahimpour, 2014] Saeed Masoudnia and Reza Ebrahimpour. Mixture of experts: a literature survey. *Artificial Intelligence Review*, 42(2):275–293, 2014.
- [Mohri *et al.*, 2012] M. Mohri, A. Rostamizadeh, and A. Talwalkar. *Foundations of machine learning*. MIT Press, 2012.
- [Morrill, 2019] J. *et al.* Morrill. The signature-based model for early detection of sepsis from electronic health records in the intensive care unit. In *CinC*, 2019.
- [Rasmus *et al.*, 2015] A. Rasmus *et al.* Semi-supervised learning with ladder networks. *arXiv:1507.02672*, 2015.
- [Reyna *et al.*, 2019] M. A Reyna *et al.* Early prediction of sepsis from clinical data: the physionet/computing in cardiology challenge. In *CinC*, 2019.
- [Silva, 2012] Ikaro *et al.* Silva. Predicting in-hospital mortality of icu patients: The physionet/computing in cardiology challenge 2012. *Computing in cardiology*, 2012.
- [Suresh *et al.*, 2018] Harini Suresh, Jen J Gong, and John V Guttag. Learning tasks for multitask learning: Heterogeneous patient populations in the icu. In *SIGKDD*, 2018.
- [V. D. Maaten and Hinton, 2008] L. V. D. Maaten and G. Hinton. Visualizing data using t-sne. *JMLR*, 9(11), 2008.
- [Xie *et al.*, 2016] J. Xie, R. Girshick, and A. Farhadi. Unsupervised deep embedding for clustering analysis. In *ICML*, pages 478–487. PMLR, 2016.
- [Yang, 2017] Bo *et al.* Yang. Towards k-means-friendly spaces: Simultaneous deep learning and clustering. In *ICML*, pages 3861–3870. PMLR, 2017.

[Zhang *et al.*, 2016] Y. Zhang, K. Lee, and H. Lee. Augmenting supervised neural networks with unsupervised objectives for large-scale image classification. In *ICML*, pages 612–621. PMLR, 2016.

[Zhao, 2015] J. et. al. Zhao. Stacked what-where auto-encoders. *arXiv preprint arXiv:1506.02351*, 2015.

A Analysis

A.1 General case

The following lemma is from [Bartlett and Mendelson, 2002; Mohri *et al.*, 2012, Theorem 3.1]:

Lemma 1. *Let \mathcal{F} be a set of maps $x \mapsto f(x)$. Suppose that $0 \leq \ell(q, y) \leq \lambda$ for any $q \in \{f(x) : f \in \mathcal{F}, x \in \mathcal{X}\}$ and $y \in \mathcal{Y}$. Then, for any $\delta > 0$, with probability at least $1 - \delta$ (over an i.i.d. draw of N i.i.d. samples $((x_i, y_i))_{i=1}^N$), the following holds: for all maps $f \in \mathcal{F}$,*

$$\mathbb{E}_{x,y}[\ell(f(x), y)] \leq \frac{1}{N} \sum_{i=1}^N \ell(f(x_i), y_i) + 2\hat{\mathcal{R}}_N(\ell \circ \mathcal{F}) + 3\lambda \sqrt{\frac{\ln(1/\delta)}{2N}}, \quad (7)$$

where $\hat{\mathcal{R}}_N(\ell \circ \mathcal{F}) := \mathbb{E}_\sigma[\sup_{f \in \mathcal{F}} \frac{1}{N} \sum_{i=1}^N \sigma_i \ell(f(x_i), y_i)]$ and $\sigma_1, \dots, \sigma_N$ are independent uniform random variables taking values in $\{-1, 1\}$.

We can use Lemma 1 to prove the following:

Theorem 2. *Let \mathcal{F}_j be a set of maps $x \in \Omega_j \mapsto f_j(x)$. Let $\mathcal{F} = \{x \mapsto f(x) : f(x) = \sum_{j=1}^K \mathbb{1}\{x \in \Omega_j\} f_j(x), f_j \in \mathcal{F}_j\}$. Suppose that $0 \leq \ell(q, y) \leq \lambda_j$ for any $q \in \{f(x) : f \in \mathcal{F}_j, x \in \Omega_j\}$ and $y \in \mathcal{Y}_j$. Then, for any $\delta > 0$, with probability at least $1 - \delta$, the following holds: for all maps $f \in \mathcal{F}$,*

$$\mathbb{E}_{x,y}[\ell(f(x), y)] \leq \sum_{j=1}^k \Pr(x \in \Omega_j) \left(\frac{1}{N_j} \sum_{i=1}^{N_j} \ell(f(x_i^j), y_i^j) + 2\hat{\mathcal{R}}_{N_j}(\ell \circ \mathcal{F}_j) + 3\lambda_j \sqrt{\frac{\ln(k/\delta)}{2N_j}} \right), \quad (8)$$

where $\hat{\mathcal{R}}_N(\ell \circ \mathcal{F}_j) := \mathbb{E}_\sigma[\sup_{f_j \in \mathcal{F}_j} \frac{1}{N} \sum_{i=1}^N \sigma_i \ell(f_j(x_i), y_i)]$ and $\sigma_1, \dots, \sigma_N$ are independent uniform random variables taking values in $\{-1, 1\}$.

Proof of Theorem 2. We have that

$$\begin{aligned} \mathbb{E}_{x,y}[\ell(f(x), y)] &= \sum_{j=1}^k \Pr(x \in \Omega_j) \mathbb{E}_{x,y}[\ell(f(x), y) \mid x \in \Omega_j] \\ &= \sum_{j=1}^k \Pr(x \in \Omega_j) \mathbb{E}_{x,y}[\ell(f_j(x), y) \mid x \in \Omega_j]. \end{aligned} \quad (9)$$

Since the conditional probability distribution is a probability distribution, we apply Lemma 1 to each term and take union bound to obtain the following: for any $\delta > 0$, with probability at least $1 - \delta$, for all $j \in \{1, \dots, k\}$ and all $f_j \in \mathcal{F}_j$,

$$\begin{aligned} \mathbb{E}_{x,y}[\ell(f_j(x), y) \mid x \in \Omega_j] &\leq \frac{1}{N_j} \sum_{i=1}^{N_j} \ell(f_j(x_i^j), y_i^j) + 2\hat{\mathcal{R}}_{N_j}(\ell \circ \mathcal{F}_j) + 3\lambda_j \sqrt{\frac{\ln(k/\delta)}{2N}} \\ &= \frac{1}{N_j} \sum_{i=1}^{N_j} \ell(f(x_i^j), y_i^j) + 2\hat{\mathcal{R}}_{N_j}(\ell \circ \mathcal{F}_j) + 3\lambda_j \sqrt{\frac{\ln(k/\delta)}{2N}}. \end{aligned}$$

Thus, using (9), we sum up both sides with the factors $\Pr(x \in \Omega_j)$ to yield:

$$\mathbb{E}_{x,y}[\ell(f(x), y)] = \sum_{j=1}^k \Pr(x \in \Omega_j) \mathbb{E}_{x,y}[\ell(f_j(x), y) \mid x \in \Omega_j] \quad (10)$$

$$\leq \sum_{j=1}^k \Pr(x \in \Omega_j) \left(\frac{1}{N_j} \sum_{i=1}^{N_j} \ell(f(x_i^j), y_i^j) + 2\hat{\mathcal{R}}_{N_j}(\ell \circ \mathcal{F}_j) + 3\lambda_j \sqrt{\frac{\ln(k/\delta)}{2N}} \right). \quad (11)$$

□

A.2 Special case: multi-class classification

For multi-class classification problems with \mathcal{B} classes and $y \in \{1, \dots, \mathcal{B}\}$, define the margin loss as follows:

$$\ell_\rho(f(x), y) = \ell_\rho^{(2)}(\ell_\rho^{(1)}(f(x), y))$$

where

$$\ell_\rho^{(1)}(f(x), y) = f(x)_y - \max_{y' \neq y} f(x)_{y'} \in \mathbb{R},$$

and

$$\ell_\rho^{(2)}(q) = \begin{cases} 0 & \text{if } \rho \leq q \\ 1 - q/\rho & \text{if } 0 \leq q \leq \rho \\ 1 & \text{if } q \leq 0. \end{cases}$$

Define the 0-1 loss as:

$$\ell_{01}(f(x), y) = \mathbb{1}\{y \neq \operatorname{argmax}_{y' \in [T]} f(x)_{y'}\},$$

where $[T] = \{1, \dots, \mathcal{B}\}$. For any $\rho > 0$, the margin loss $\ell_\rho(f(x), y)$ is an upper bound on the 0-1 loss: i.e., $\ell_\rho(f(x), y) \geq \ell_{01}(f(x), y)$.

The following lemma is from [Mohri *et al.*, 2012, Theorem 8.1]:

Lemma 2. *Let \mathcal{F} be a set of maps $x \mapsto f(x)$. Fix $\rho > 0$. Then, for any $\delta > 0$, with probability at least $1 - \delta$ over an i.i.d. draw of N i.i.d. test samples $((x_i, y_i))_{i=1}^m$, the following holds: for all maps $f \in \mathcal{F}$,*

$$\mathbb{E}_{x,y}[\ell_{01}(f(x), y)] \leq \frac{1}{N} \sum_{i=1}^N \ell_\rho(f(x_i), y_i) + \frac{2\mathcal{B}^2}{\rho} \hat{\mathcal{R}}_N(\mathcal{F}_\mathcal{B}) + \left(1 + \frac{2\mathcal{B}^2}{\rho}\right) \sqrt{\frac{\ln(2/\delta)}{2N}},$$

where $\mathcal{F}_\mathcal{B} = \{x \mapsto f(x)_k : f \in \mathcal{F}, k \in [T]\}$.

Proof. Using Theorem 8.1 [Mohri *et al.*, 2012], we have that with probability at least $1 - \delta/2$,

$$\mathbb{E}_{x,y}[\ell_{01}(f(x), y)] \leq \frac{1}{N} \sum_{i=1}^N \ell_\rho(f(x_i), y_i) + \frac{2\mathcal{B}^2}{\rho} \mathcal{R}_N(\mathcal{F}_\mathcal{B}) + \sqrt{\frac{\ln(2/\delta)}{2N}},$$

Since changing one point in S changes $\hat{\mathcal{R}}_m(\mathcal{F}_\mathcal{B})$ by at most $1/N$, McDiarmid's inequality implies the statement of this lemma by taking union bound. \square

Theorem 3. *Let \mathcal{F}_j be a set of maps $x \in \Omega_j \mapsto f_j(x)$. Let $\mathcal{F} = \{x \mapsto f(x) : f(x) = \sum_{j=1}^k \mathbb{1}\{x \in \Omega_j\} f_j(x), f_j \in \mathcal{F}_j\}$. Suppose that $0 \leq \ell(q, y) \leq \lambda_j$ for any $q \in \{f(x) : f \in \mathcal{F}_j, x \in \Omega_j\}$ and $y \in \mathcal{Y}_j$. Then, for any $\delta > 0$, with probability at least $1 - \delta$, the following holds: for all maps $f \in \mathcal{F}$,*

$$\mathbb{E}_{x,y}[\ell_{01}(f(x), y)] \leq \sum_{j=1}^k \Pr(x \in \Omega_j) \left(\frac{1}{N_j} \sum_{i=1}^{N_j} \ell_\rho(f(x_i^j), y_i^j) + \frac{2\mathcal{B}^2}{\rho} \hat{\mathcal{R}}_{N_j}(\mathcal{F}_{T,j}) + \left(1 + \frac{2\mathcal{B}^2}{\rho}\right) \sqrt{\frac{\ln(2k/\delta)}{2N_j}} \right), \quad (12)$$

where $\hat{\mathcal{R}}_{N_j}(\mathcal{F}_{T,j}) := \mathbb{E}_\sigma[\sup_{f_j \in \mathcal{F}_{T,j}} \frac{1}{N} \sum_{i=1}^{N_j} \sigma_i \ell(f_j(x_i^j), y_i^j)]$ and $\sigma_1, \dots, \sigma_N$ are independent uniform random variables taking values in $\{-1, 1\}$. Here, $\mathcal{F}_{\mathcal{B},j} = \{x \mapsto f(x)_k : f \in \mathcal{F}_j, k \in [\mathcal{B}]\}$.

Proof of Theorem 2. We have that

$$\begin{aligned} \mathbb{E}_{x,y}[\ell_{01}(f(x), y)] &= \sum_{j=1}^K \Pr(x \in \Omega_j) \mathbb{E}_{x,y}[\ell_{01}(f(x), y) \mid x \in \Omega_j] \\ &= \sum_{j=1}^k \Pr(x \in \Omega_j) \mathbb{E}_{x,y}[\ell_{01}(f_j(x), y) \mid x \in \Omega_j]. \end{aligned} \quad (13)$$

Since the conditional probability distribution is a probability distribution, we apply Lemma 1 to each term and take union bound to obtain the following: for any $\delta > 0$, with probability at least $1 - \delta$, for all $j \in \{1, \dots, k\}$ and all $f_j \in \mathcal{F}_j$,

$$\begin{aligned} \mathbb{E}_{x,y}[\ell_{01}(f_j(x), y) \mid x \in \Omega_j] &\leq \frac{1}{N_j} \sum_{i=1}^{N_j} \ell_\rho(f_j(x_i^j), y_i^j) + \frac{2\mathcal{B}^2}{\rho} \hat{\mathcal{R}}_{N_j}(\mathcal{F}_{\mathcal{B},j}) + \left(1 + \frac{2\mathcal{B}^2}{\rho}\right) \sqrt{\frac{\ln(2k/\delta)}{2N}} \\ &= \frac{1}{N_j} \sum_{i=1}^{N_j} \ell_\rho(f(x_i^j), y_i^j) + \frac{2\mathcal{B}^2}{\rho} \hat{\mathcal{R}}_{N_j}(\mathcal{F}_{\mathcal{B},j}) + \left(1 + \frac{2\mathcal{B}^2}{\rho}\right) \sqrt{\frac{\ln(2k/\delta)}{2N}}. \end{aligned}$$

Thus, using (13), we sum up both sides with the factors $\Pr(x \in \Omega_j)$ to yield:

$$\begin{aligned} \mathbb{E}_{x,y}[\ell_{01}(f(x), y)] &= \sum_{j=1}^k \Pr(x \in \Omega_j) \mathbb{E}_{x,y}[\ell_{01}(f_j(x), y) \mid x \in \Omega_j] \\ &\leq \sum_{j=1}^k \Pr(x \in \Omega_j) \left(\frac{1}{N_j} \sum_{i=1}^{N_j} \ell_\rho(f(x_i^j), y_i^j) + \frac{2\mathcal{B}^2}{\rho} \hat{\mathcal{R}}_{N_j}(\mathcal{F}_{\mathcal{B},j}) + \left(1 + \frac{2\mathcal{B}^2}{\rho}\right) \sqrt{\frac{\ln(2k/\delta)}{2N}} \right). \end{aligned} \quad (14)$$

□

A.3 Special case: deep neural networks with binary classification

Note that for any $\rho > 0$, the margin loss $\ell_\rho(f(x), y)$ is an upper bound on the 0-1 loss: i.e., $\ell_\rho(f(x), y) \geq \ell_{01}(f(x), y)$.

The following lemma is from [Mohri *et al.*, 2012, Theorem 4.4]:

Lemma 3. *Let \mathcal{F} be a set of real-valued functions. Fix $\rho > 0$. Then, for any $\delta > 0$, with probability at least $1 - \delta$ over an i.i.d. draw of m i.i.d. test samples $((x_i, y_i))_{i=1}^m$, the following holds: for all maps $f \in \mathcal{F}$,*

$$\mathbb{E}_{x,y}[\ell_{01}(f(x), y)] \leq \frac{1}{m} \sum_{i=1}^m \ell_\rho(f(x_i), y_i) + \frac{2}{\rho} \hat{\mathcal{R}}_m(\mathcal{F}) + 3\sqrt{\frac{\ln(2/\delta)}{2m}}.$$

Theorem 4. *Let \mathcal{F}_j be a set of maps $x \in \Omega_j \mapsto f_j(x)$. Let $\mathcal{F} = \{x \mapsto f(x) : f(x) = \sum_{j=1}^K \mathbb{1}\{x \in \Omega_j\} f_j(x), f_j \in \mathcal{F}_j\}$. Suppose that $0 \leq \ell(q, y) \leq \lambda_j$ for any $q \in \{f(x) : f \in \mathcal{F}_j, x \in \Omega_j\}$ and $y \in \mathcal{Y}_j$. Then, for any $\delta > 0$, with probability at least $1 - \delta$, the following holds: for all maps $f \in \mathcal{F}$,*

$$\mathbb{E}_{x,y}[\ell_{01}(f(x), y)] \leq \sum_{j=1}^k \Pr(x \in \Omega_j) \left(\frac{1}{N_j} \sum_{i=1}^{N_j} \ell_\rho(f(x_i^j), y_i^j) + \frac{2}{\rho} \hat{\mathcal{R}}_{N_j}(\mathcal{F}_j) + 3\sqrt{\frac{\ln(2/\delta)}{2N_j}} \right), \quad (16)$$

where $\hat{\mathcal{R}}_{N_j}(\mathcal{F}_j) := \mathbb{E}_\sigma[\sup_{f_j \in \mathcal{F}_j} \frac{1}{N} \sum_{i=1}^{N_j} \sigma_i \ell(f_j(x_i^j), y_i^j)]$ and $\sigma_1, \dots, \sigma_N$ are independent uniform random variables taking values in $\{-1, 1\}$.

Proof of Theorem 4. We have that

$$\begin{aligned} \mathbb{E}_{x,y}[\ell_{01}(f(x), y)] &= \sum_{j=1}^k \Pr(x \in \Omega_j) \mathbb{E}_{x,y}[\ell_{01}(f(x), y) \mid x \in \Omega_j] \\ &= \sum_{j=1}^K \Pr(x \in \Omega_j) \mathbb{E}_{x,y}[\ell_{01}(f_j(x), y) \mid x \in \Omega_j]. \end{aligned} \quad (17)$$

Since the conditional probability distribution is a probability distribution, we apply Lemma 3 to each term and take union bound to obtain the following: for any $\delta > 0$, with probability at least $1 - \delta$, for all $j \in \{1, \dots, k\}$ and all $f_j \in \mathcal{F}_j$,

$$\begin{aligned} \mathbb{E}_{x,y}[\ell_{01}(f_j(x), y) \mid x \in \Omega_j] &\leq \frac{1}{N_j} \sum_{i=1}^{N_j} \ell_\rho(f_j(x_i^j), y_i^j) + \frac{2}{\rho} \hat{\mathcal{R}}_{N_j}(\mathcal{F}_j) + 3\sqrt{\frac{\ln(2/\delta)}{2N_j}} \\ &= \frac{1}{N_j} \sum_{i=1}^{N_j} \ell_\rho(f(x_i^j), y_i^j) + \frac{2}{\rho} \hat{\mathcal{R}}_{N_j}(\mathcal{F}_j) + 3\sqrt{\frac{\ln(2/\delta)}{2N_j}}. \end{aligned}$$

Thus, using (17), we sum up both sides with the factors $\Pr(x \in \Omega_j)$ to yield:

$$\mathbb{E}_{x,y}[\ell_{01}(f(x), y)] = \sum_{j=1}^K \Pr(x \in \Omega_j) \mathbb{E}_{x,y}[\ell_{01}(f_j(x), y) \mid x \in \Omega_j] \quad (18)$$

$$\leq \sum_{j=1}^k \Pr(x \in \Omega_j) \left(\frac{1}{N_j} \sum_{i=1}^{N_j} \ell_\rho(f(x_i^j), y_i^j) + \frac{2}{\rho} \hat{\mathcal{R}}_{N_j}(\mathcal{F}_j) + 3\sqrt{\frac{\ln(2/\delta)}{2N_j}} \right). \quad (19)$$

□

We are now ready to prove Theorem 1.

Proof of Theorem 1. Using Theorem 4 with $\Pr(x \in \Omega_j) = 1/k$ and $m_j = N/k$, for $f \in \mathcal{F}^k$,

$$\begin{aligned}
\mathbb{E}_{x,y}[\ell_{01}(f(x), y)] &\leq \frac{1}{k} \sum_{j=1}^k \left(\frac{1}{(N/k)} \sum_{i=1}^{N/k} \ell_{\rho}(f(x_i^j), y_i^j) + 2\rho^{-1} \hat{\mathcal{R}}_{N/k}(\mathcal{F}_j) + 3\sqrt{\frac{\ln(2/\delta)}{2(N/k)}} \right) \\
&= \frac{1}{k} \sum_{j=1}^k \left(\frac{k}{N} \sum_{i=1}^{N/k} \ell_{\rho}(f(x_i^j), y_i^j) + 2\rho^{-1} \hat{\mathcal{R}}_{N/k}(\mathcal{F}_j) + 3\sqrt{\frac{k \ln(2k/\delta)}{2N}} \right) \\
&= \frac{1}{N} \sum_{j=1}^k \sum_{i=1}^{N/k} \ell_{\rho}(f(x_i^j), y_i^j) + \frac{2\rho^{-1}}{k} \sum_{j=1}^k \hat{\mathcal{R}}_{N/k}(\mathcal{F}_j) + 3\sqrt{\frac{k \ln(2k/\delta)}{2N}} \\
&= \hat{\mathbb{E}}_{x,y}[\ell_{\rho}(f(x), y)] + \frac{2\rho^{-1}}{k} \sum_{j=1}^k \hat{\mathcal{R}}_{N/k}(\mathcal{F}_j) + 3\sqrt{\frac{k \ln(2k/\delta)}{2N}}
\end{aligned}$$

Here, using Theorem 1 of [Golowich *et al.*, 2018], we have that

$$\hat{\mathcal{R}}_{N/k}(\mathcal{F}_j) \leq \frac{B_j \sqrt{k} (\sqrt{2 \log(2)(L+Q)} + 1) (\prod_{l=1}^L M_l^j) (\prod_{l=1}^Q M_l^0)}{\sqrt{N}}.$$

Thus, for any $\delta > 0$, with probability at least $1 - \delta$ over an i.i.d. draw of N i.i.d. test samples $((x_i, y_i))_{i=1}^N$, the following holds: for all maps $f \in \mathcal{F}^K$,

$$\begin{aligned}
&\mathbb{E}_{x,y}[\ell_{01}(f(x), y)] - \hat{\mathbb{E}}_{x,y}[\ell_{\rho}(f(x), y)] \\
&\leq \frac{2\rho^{-1}}{K} \sum_{j=1}^K \frac{B_j \sqrt{k} (\sqrt{2 \log(2)(L+Q)} + 1) (\prod_{l=1}^L M_l^j) (\prod_{l=1}^Q M_l^0)}{\sqrt{N}} + 3\sqrt{\frac{k \ln(2k/\delta)}{2N}} \\
&\leq \frac{2\rho^{-1} (\sqrt{2 \log(2)(L+Q)} + 1) (\prod_{l=1}^Q M_l^0) \left(\sum_{j=1}^k B_j \prod_{l=1}^L M_l^j \right)}{\sqrt{kN}} + 3\sqrt{\frac{k \ln(2k/\delta)}{2N}}
\end{aligned}$$

□

By taking union bound over M_l^j , it is straightforward to replace $\prod_{l=1}^L M_l^j$ by $\prod_{l=1}^L \|W_l^j\|_F$ in the bound of Theorem 1 with additional factors that is not dominant and hidden in the \tilde{O} notation (see the proof of Lemma A.9 of [Bartlett *et al.*, 2017] or the proof of Theorem 2 of [Koltchinskii and Panchenko, 2002]).

B Extended Results

Dataset	k	SIL				
		KMeans	DCN	IDEC	DMNN	EXPERTNET
CIC	2	0.54	NA	0.51	0.125	0.358
	3	0.297	NA	0.354	0.092	0.305
	4	0.168	NA	0.326	0.085	0.231
Sepsis	2	0.588	0.253	0.325	0.250	0.357
	3	0.277	0.242	0.406	0.104	0.349
	4	0.212	NA	0.307	0.099	0.248
AKI	2	0.401	0.596	0.769	0.259	0.638
	3	0.459	0.782	0.828	0.285	0.611
	4	0.459	0.585	0.622	0.278	0.53
ARDS	2	0.369	0.65	0.746	0.295	0.484
	3	0.384	NA	0.553	0.319	0.628
	4	0.4	NA	0.856	0.301	0.76
WID-M	2	0.346	0.797	0.423	0.202	0.393
	3	0.189	NA	0.45	0.157	0.282
	4	0.136	NA	0.544	0.152	0.197
Diabetes	2	0.249	0.448	0.378	0.156	0.129
	3	0.201	0.181	0.503	0.167	0.154
	4	0.157	0.088	0.423	0.183	0.24
CIC.LOS	2	0.547	0.582	0.546	-	0.231
	3	0.306	0.372	0.447	-	0.099
	4	0.162	NA	0.349	-	0.129

Table 4: Silhouette Scores. Best values in bold.

F1								
Dataset	k	Baseline	SAE	KMeans-Z	DCN-Z	IDEC-Z	DMNN-Z	EXPERTNET
CIC	1	0.436	0.487	0.617	0.629	0.628	0.299	0.678
	2			0.639	NA	0.569	0.379	0.712
	3			0.597	NA	0.606	0.413	0.693
	4			0.432	NA	0.582	0.404	0.708
Sepsis	1	0.500	0.498	0.715	0.646	0.684	0.157	0.806
	2			0.561	0.525	0.686	0.427	0.822
	3			0.557	0.59	0.653	0.363	0.814
	4			0.504	NA	0.612	0.537	0.815
AKI	1	0.506	0.417	0.57	0.528	0.578	0.382	0.638
	2			0.333	0.529	0.527	0.645	0.642
	3			0.459	0.569	0.541	0.647	0.625
	4			0.361	0.571	0.574	0.640	0.605
ARDS	1	0.481	0.481	0.561	0.529	0.525	0.043	0.554
	2			0.499	0.498	0.483	0.132	0.567
	3			0.555	NA	0.492	0.143	0.564
	4			0.548	NA	0.481	0.163	0.551
WID-M	1	0.520	0.514	0.644	0.581	0.65	0.026	0.696
	2			0.604	0.497	0.621	0.331	0.694
	3			0.582	NA	0.616	0.331	0.686
	4			0.578	NA	0.606	0.360	0.686
Diabetes	1	0.471	0.438	0.491	0.436	0.486	0.226	0.465
	2			0.438	0.421	0.468	0.235	0.493
	3			0.468	0.401	0.439	0.280	0.447
	4			0.453	0.393	0.451	0.279	0.46
CIC-LOS	1	0.399	0.427	0.433	0.403	0.431	-	0.458
	2			0.354	0.371	0.409	-	0.456
	3			0.324	0.394	0.403	-	0.46
	4			0.292	NA	0.398	-	0.442

Table 5: F1 Scores. Best values in bold.

C Extended Ablation Analysis

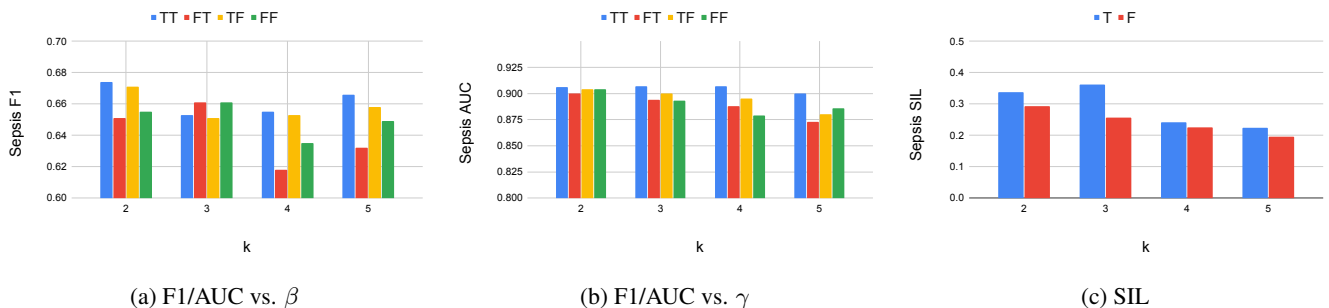


Figure 3: Ablation study on Sepsis dataset. TT represents that stochastic sampling is turned on in both training and testing phase. Similarly for other combinations. Note that stochastic sampling turned on in the training phase has a strong effect on performance.

D Data Preprocessing and Feature Extraction

We evaluate the results on 6 real world clinical datasets out of which 3 are derived from the MIMIC III dataset derived from Beth Israel Deaconess Hospital. CIC dataset is derived from 2012 Physionet challenge [Silva, 2012] of predicting in-hospital

mortality of intensive care units. The Sepsis dataset is derived from the 2019 Physionet challenge of sepsis onset prediction. We manually extract the Acute Kidney Failure (AKI) and Acute Respiratory Distress Syndrome (ARDS) datasets from the larger MIMIC III dataset. WID Mortality dataset is extracted from the 2020 Women In Data Science challenge to predict patient mortality. The Diabetes Readmission prediction dataset consists of 100000 records of patients. This is a multiclass version of the CIC dataset where the Length of Stay (LOS) feature is discretized into 3 classes using quartiles. The task is to predict the LOS of ICU patients.

- **CIC:** The CIC dataset is derived from the 2012 Physionet challenge [Silva, 2012] of predicting in-hospital mortality of intensive care units (ICU) patients at the end of their hospital stay. The data has time-series records, comprising various physiological parameters of 12000 patient ICU stays. We follow the data processing scheme of [Johnson, 2012] (the top ranked team in the competition) to obtain static 117-dimensional features for each patient.
- **Sepsis:** The Sepsis dataset is derived from the 2019 Physionet challenge of sepsis onset prediction. The dataset has time-series records, comprising various physiological parameters of ~ 40000 patients. We follow the data processing scheme of the competition winners [Morrill, 2019] to obtain static 89 dimensional features for each patient.
- **AKI and ARDS:** We manually extract the Acute Kidney Failure (AKI) and Acute Respiratory Distress Syndrome (ARDS) datasets from the larger MIMIC III dataset. We follow the KDIGO criteria to determine kidney failure onset time and the Berlin criteria for ARDS. The challenge is to predict kidney failure onset ahead of time. Similar to the above datasets, we derive static vectors from the time series data.
- **WID Mortality:** This dataset is extracted from the 2020 Women In Data Science challenge where the objective is to create a model that uses data from the first 24 hours of intensive care to predict patient survival. We perform standard data cleaning procedures before using the dataset.
- **Diabetes:** The Diabetes Readmission prediction dataset consists of 100000 records of patients from 130 hospitals in the US from the year 1998 to 2008.
- **CIC-LOS:** This is a multiclass version of the CIC dataset where the Length of Stay (LOS) feature is discretized into 3 classes using quartiles. The task is to predict the LOS of ICU patients.

E EXPERTNET Optimization Details

E.1 Updating EXPERTNET parameters

Optimizing $(\mathcal{U}, \mathcal{V})$ is similar to training an SAE - but with the additional loss terms L_c, L_s and L_{bal} . We code our algorithm in PyTorch which allows us to easily backpropagate all the losses simultaneously. To implement SGD for updating the network parameters, we look at the problem w.r.t. the incoming data x_i :

$$\begin{aligned} \min_{\mathcal{U}, \mathcal{W}} L^i &= \ell(g(f(x_i)), x_i) + \beta \cdot \text{KL}(P, Q) \\ &+ \gamma \cdot \sum_{j=1}^k q_{i,j} \text{CE}(y_i, h_j(x_i; \mathcal{V}_j)) + \delta \cdot L_{bal} \end{aligned}$$

The gradient of the above function over the network parameters is easily computable. Let $\mathcal{J} = (\mathcal{U}, \mathcal{V}, \mathcal{W})$ be the collection of network parameters, then for a fixed target distribution P , the gradients of L_c w.r.t. embedded point z_i and cluster center μ_j can be computed as:

$$\begin{aligned} \frac{\partial L_c}{\partial z_i} &= 2 \sum_{j=1}^k \left(1 + \|z_i - \mu_j\|^2\right)^{-1} (p_{ij} - q_{ij}) (z_i - \mu_j) \\ \frac{\partial L_c}{\partial \mu_j} &= 2 \sum_i \left(1 + \|z_i - \mu_j\|^2\right)^{-1} (q_{ij} - p_{ij}) (z_i - \mu_j) \end{aligned}$$

The above derivations are from [Xie *et al.*, 2016]. We leverage the power of automatic differentiation to calculate the gradients of L_{bal} and L_s during execution. Then given a mini batch with m samples and learning rate λ , μ_j is updated by:

$$\mu_j = \mu_j - \frac{\tau}{m} \sum_{i=1}^m \frac{\partial L_c}{\partial \mu_j} \quad (20)$$

The decoder's weights are updated by:

$$\mathcal{V} = \mathcal{V} - \frac{\tau}{m} \sum_{i=1}^m \frac{\partial L_r}{\partial \mathcal{V}} \quad (21)$$

and the encoder’s weights are updated by:

$$\mathcal{U} = \mathcal{U} - \frac{\tau}{m} \sum_{i=1}^m \left(\frac{\partial L_r}{\partial \mathcal{U}} + \beta \frac{\partial L_c}{\partial \mathcal{U}} + \gamma \frac{\partial L_s}{\partial \mathcal{U}} + \delta \frac{\partial L_{bal}}{\partial \mathcal{U}} \right) \quad (22)$$

$$\mathcal{J} \leftarrow \mathcal{J} - \tau \nabla_{\mathcal{J}} L^i$$

where τ is the diminishing learning rate.

F Case Study: Additional Analysis

Cluster 1	Cluster 2	Cluster 3
SAPS-I	Length_of_stay	SAPS-I
SOFA	CCU	SOFA
GCS_first	CSRU	Length_of_stay
GCS_lowest	DiasABP_first	Weight
CSRU	GCS_first	CSRU
Creatinine_last	Creatinine_last	MechVentLast8Hour
Creatinine_last	Glucose_first	DiasABP_first
GCS_last	HR_first	Glucose_first
BUN_last	MAP_first	HR_first
Creatinine_first	NIDiasABP_first	MAP_first
Lactate_first	NIMAP_first	NIDiasABP_first

Table 6: Cluster wise features sorted by HTFD values.

We study the clusters found by EXPERTNET by analyzing the HTFD metric in table 6. SAPS-I and SOFA have high HTFD in clusters 1 and 3. This indicates that the two clusters have different distributions of SAPS-I and SOFA. It (SOFA) is also an important feature for cluster 3’s risk model (Table 3) but in distribution, it is similar to SOFA values of clusters 2 but not 1. GCS_Last (Glasgow Coma Score) is an important feature for all the three risk models but not significantly different across the three clusters (cluster averages 12.744, 14.489, 10.226). Normal GCS is 15.